Acta Crystallographica Section B
Structural Science, Crystal Engineering and Materials
ISSN 2052-5192

Weak intermolecular hydrogen and halogen interactions in an isomorphous halogen series of pseudoterpyridine Zn^{II} complexes

Florina Dumitru,[a,b] Yves-Marie Legrand,[a] Mihail Barboiu[a]* and Arie van der Lee[a]*

[a]Institut Européen des Membranes, ENSCM-UMII-CNRS, Place Eugène Bataillon, Montpellier 34095, France, and [b]Department of Inorganic Chemistry, University 'Politehnica' of Bucharest, 1 Polizu st., Bucharest 011061, Romania

Correspondence e-mail: mihail-dumitru.barboiu@univ-montp2.fr, avderlee@univ-montp2.fr

Received 2 November 2012
Accepted 11 December 2012

The synthesis and characterization of a series of halogen-substituted pseudoterpyridine Zn^{II} homoleptic mononuclear complexes, based on ligands L_{11}–L_{44} [2,6-pyridinedicarboxaldehydebis(*p*-*R*-phenylimines), *R* = F, Cl, Br, I] are reported. Neither of the structures contain relatively strong classical hydrogen bonds (OH···O, NH···O, OH···N, NH···N) and the structure packing is thus determined by a subtle interplay of weaker interactions. Isostructurality of the four halogen analogues is very rare, and in this study —Br, —Cl and —F are found to be isostructural in different degrees, whereas —I is not. Interestingly, although it is closely isostructural to the —Cl and —Br compounds, the F analogue is shown not to form F···O bonds, while the Cl and the Br analogues do form Hal···O bonds. This raises an important question on the role of Hal···O bonds in the structuration of the crystal packing, particularly the stabilization effect. Similarly, while the CH···Hal interaction seems to give one-dimensional cohesion in the —Cl and —Br analogues, this feature is absent in the —F analogue, despite its close isostructurality. CH···O interactions appear to dominate to a first degree the cohesion between the anionic trifluoromethanesulfonate network and the cationic Zn-pyridinedicarboxaldehydebis(*p*-*R*-phenylimines) network. The analysis of these interactions is corroborated by reduced density gradient calculations based on promolecular densities.

1. Introduction

Halogen bonding, a weak intermolecular interaction, is an effective and reliable tool in solid-state supramolecular chemistry as described by Metrangolo & Resnati (2001) and Metrangolo *et al.* (2008), opening new perspectives in materials design and supramolecular synthesis (Meyer & Dubois, 2013). In recent years, halogen bonding ($X\cdots B$) has proven to be a very attractive tool in the design of functional self-assembled architectures such as liquid crystals (Nguyen *et al.*, 2004; Metrangolo *et al.*, 2006; Präsang *et al.*, 2008), nonlinear optical (Cariati *et al.*, 2007) or magnetic/conductive materials (Fourmigué & Batail, 2004; Fourmigué, 2008), anion sensors (Metrangolo *et al.*, 2009; Cavallo *et al.*, 2010), catalytic systems (Bruckmann *et al.*, 2008; Walter *et al.*, 2011) amongst other recently discovered halogen bonding functional materials. Equally important, halogen-bonding ($X\cdots B$) based recognition processes are of relevant interest in biological systems, due to their role in the stabilization of complexes between small halogen-substituted ligands and biological substrates (*i.e.* ligand–protein interaction). Halogen bonding of halogen-type compounds (*e.g.* triclosan, halothane, HIV-1 reverse transcriptase inhibitors *etc.*) with proteins provides valuable information on the nature of specific and highly directional

interactions for drug design (Parisini *et al.*, 2011). From a structural point of view, halogen bonds in which the halogen atom is the electron acceptor are closely related to hydrogen bonds, as in both types of bonding an electron donor/electron acceptor relationship exists. With strengths ranging from 5 to 180 kJ mol^{-1} (the strength of the interaction increases in the order Cl < Br < I, following the polarizability of the halogen atom) and the high directionality of interactions, halogen bonding competes with hydrogen bonding (generally slightly weaker) as supramolecular self-assembly motifs or as crystal engineering scaffolds (Rissanen, 2008). The behavior of halogens, F, Cl, Br and I, in halogen bonding has been attributed to the anisotropic (non-spherical) charge distribution in halogen atoms (Gonnade *et al.*, 2007; Raatikainen *et al.*, 2010; Politzer *et al.*, 2012). Heavier halogens (except fluorine, due to extreme electronegativity and limited polarizability) exhibit electrophilic character along the axis of C—*X* bonds and nucleophilic character perpendicular to these bonds; electrophiles in general tend to approach halogens at angles of *ca* 100° and nucleophiles at 165° (Gonnade *et al.*, 2007). The stronger the electron-withdrawing environment around the halogen atoms, the higher their ability to be engaged in halogen-bonding interactions.

This study is part of a larger project where the design and construction of metallosupramolecular architectures are based on the implementation of ligands in which specific molecular information can be embedded in lateral aromatic arms reversibly connected to a pseudoterpyridine metal coordination center [see Scheme (I)].

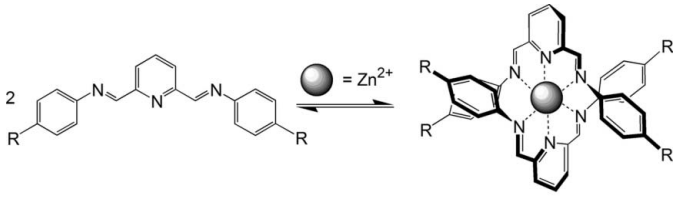

L11, R= F
L22, R= Cl
L33, R= Br
L44, R= I

(**L11**)$_2$Zn^{II}, R= F
(**L22**)$_2$Zn^{II}, R= Cl
(**L33**)$_2$Zn^{II}, R= Br
(**L44**)$_2$Zn^{II}, R= I

(I)

Metal centers and the nature of the arms of the ligands forming the complex can be varied. Diverse metallosupramolecular combinatorial libraries can easily be generated by simply mixing a metal ion with different ligands (Legrand *et al.*, 2007; Lehn, 1999; Kramer *et al.*, 1993; Barboiu, 2010; Brady & Sanders, 1997; Storm & Luning, 2002; Goral *et al.*, 2001; Choudhary & Morrow, 2002; Dumitru *et al.*, 2005; Barboiu, Petit *et al.*, 2006; Barboiu, Ruben *et al.*, 2006). The constitutional self-organization into metallosupramolecular architectures around a metal ion center might be related to direct suitable ligands by reading out the structural information (intrinsic information – electronic and steric factors, *i.e.* donor atom type, number and spatial distribution of binding sites) of the ligands through an algorithm defined by their *inner* coordination geometry and *outer* supramolecular/constitutional requirements (Barboiu *et al.*, 2009; Dumitru *et al.*, 2009; Barboiu, 2012). Most of these examples have been targeted to pseudoterpyridine ligands [2,6-pyridinedicarboxaldehydebis(*p*-substituted-phenylimines)] which similarly coordinate octahedral metal ions (Zn^{II}, Fe^{II}, Co^{II}, Pb^{II}) and organize the ligands into a mutually orthogonal orientation. In this contribution we focus both on the preparation of the metallosupramolecular complexes of Zn^{II} and the halogeno-pseudoterpyridine-type ligands L_{11}–L_{44} [2,6-pyridinedicarboxaldehydebis(*p*-*R*-phenylimines), *R* = F, Cl, Br, I, denoted hereafter as PDA-*R*] in the presence of $CF_3SO_3^-$ (trifluoromethanesulfonate) counterions [Scheme (I)] and on the study of their crystallographic similarities and differences by a detailed analysis of the role of halogen atoms in the crystal packing both as an acceptor and donor. The structures do not contain 'classical' hydrogen bonds (OH···O, NH···O, OH···N, NH···N), but only weak interactions involving halogen and H atoms besides a number of CH···π interactions, which makes them particularly attractive to study the influence of these interactions on the crystal packing.

2. Experimental

2.1. Materials and methods

2,6-Pyridinedicarboxaldehyde was prepared by oxidation of 2,6-pyridinemethanol with activated MnO_2 according to the procedure described in the literature (Vance *et al.*, 1998). 4-Fluoroaniline, 4-chloroaniline, 4-bromoaniline, 4-iodoaniline and $Zn(CF_3SO_3)_2$ were purchased from Aldrich and used as received. All other reagents were obtained from commercial suppliers and used without further purification. All organic solutions were routinely dried by using sodium sulfate (Na_2SO_4). ^{1}H and ^{13}C NMR spectra were recorded on an ARX 300 MHz Bruker spectrometer in $CDCl_3$ and CD_3CN with the use of the residual solvent peak as a reference. Mass spectrometric studies were performed in the positive ion mode using a quadrupole mass spectrometer (Micromass, Platform II). Samples were continuously introduced into the mass spectrometer through a Waters 616HPLC pump. The temperature (353 K) and the extraction cone voltage (V_c = 5–10 V) were usually set to avoid excessive fragmentations.

2.2. General procedure for the synthesis of ligands L_{11}–L_{44}

The synthesis of bis(2,6-pyridinedicarboxaldehydebis(*p*-fluorophenylimine)), L_{11}, was reported by us recently (Dumitru *et al.*, 2009). The ligands L_{22}–L_{44} are not described in the literature and they have been synthesized as follows: L_{22}–L_{44} have been synthesized in EtOH by condensation of 1 equiv. of 2,6-pyridinedicarboxaldehyde (0.1 g, 0.74 mmol) with 2 equiv. of 4-haloaniline (1.48 mmol), under reflux for 24 h with constant stirring. After solvent evaporation, the resulting crude materials were recrystallized from diethyl ether to give the title compounds as light-yellow, white-yellow and yellow solids.

2.2.1. 2,6-Pyridinedicarboxaldehydebis(*p*-fluorophenylimine), L_{11}. $C_{19}H_{13}F_2N_3$, *MW* = 321.32 g mol^{-1}; ^{1}H NMR (300 Hz, $CDCl_3$, p.p.m.): δ 8.660 (s, 2H, CH═N), 8.284–8.258

(d, 2H, H^b, J = 7.8 Hz), 7.972–7.920 (t, 1H, H^a, J = 7.8 Hz), 7.316–7.300 (m, 4H, H^c), 7.176–7.108 (d, 4H, H^d). The ^{1}H NMR spectrum is displayed in Fig. S1 of the supplementary material.[1]

2.2.2. 2,6-Pyridinedicarboxaldehydebis(*p*-chlorophenylimine), L_{22} (0.197 g, yield 75%). $C_{19}H_{13}Cl_2N_3$, MW = 354.24 g mol^{-1}. ^{1}H NMR (300 MHz, $CDCl_3$, p.p.m.): δ 8.651 (s, 2H, CH═N), 8.296–8.270 (d, 2H, H^b, J = 7.8 Hz), 7.986–7.935 (t, 1H, H^a, J = 7.8 Hz), 7.415–7.386 (dd, 4H, H^d, J = 8.7 Hz), 7.277–7.247 (dd, 4H, H^c, J = 9 Hz). The ^{1}H NMR spectrum is displayed in Fig. S2.

2.2.3. 2,6-Pyridinedicarboxaldehydebis(*p*-bromophenylimine), L_{33} (0.262 g, yield 80%). $C_{19}H_{13}Br_2N_3$, MW = 443.14 g mol^{-1}. ^{1}H NMR (300 MHz, $CDCl_3$, p.p.m.): δ 8.634 (s, 2H, CH═N), 8.283–8.257 (d, 2H, H^b, J = 7.8 Hz), 7.973–7.921 (t, 1H, H^a, J = 7.8 Hz), 7.550–7.524 (dd, 4H, H^d, J = 7.8 Hz), 7.198–7.171 (dd, 4H, H^c, J = 8.1 Hz). The ^{1}H NMR spectrum is displayed in Fig. S3.

2.2.4. 2,6-Pyridinedicarboxaldehydebis(*p*-iodophenylimine), L_{44} (0.33 g, yield 83%). $C_{19}H_{13}I_2N_3$, MW = 537.14 g mol^{-1}.^{1}H NMR (300 MHz, $CDCl_3$, p.p.m.): δ 8.637 (s, 2H, CH═N), 8.292–8.266 (d, 2H, H^b, J = 7.8 Hz), 7.981–7.929 (t, 1H, H^a, J = 7.8 Hz), 7.761–7.732 (dd, 4H, H^d, J = 8.7 Hz), 7.079–7.051 (dd, 4H, H^c, J = 8.4 Hz). The ^{1}H NMR spectrum is displayed in Fig. S4.

2.3. Synthesis of $[Zn(L_{11})_2]^{II}$–$[Zn(L_{44})_2]^{II}$ complexes

The reactions were performed typically on a 10 mg scale of ligand. The ligands L_{11}–L_{44} and $Zn(CF_3SO_3)_2$ (molar ratio ligand–metal 2:1) were dissolved in CD_3CN (1 ml), and stirred overnight at 333 K. Layering such solutions of duplex complexes $[Zn(L_{11})_2]^{II}$–$[Zn(L_{44})_2]^{II}$ in acetonitrile with isopropyl ether or benzene at room temperature resulted in single crystals suitable for X-ray single-crystal experiments.

2.3.1. Complex $[Zn(L_{11})_2]^{II}$. ^{1}H NMR (300 MHz, CD_3CN, p.p.m.): δ 8.775 (s, 4H, CH═N), 8.628–8.575 (t, 2H, H^a, J = 8.1, 7.8 Hz), 8.290–8.264 (d, 4H, H^b, J = 7.8 Hz), 7.034–6.976 (m, 8H, H^c, J = 8.7 Hz), 6.813–6.767 (m, 8H, H^d). MS (ESI): m/z (%): 353.5 (100) $[Zn(L_{11})_2]^{II}$. The ^{1}H NMR spectrum is displayed in Fig. S5.

2.3.2. Complex $[Zn(L_{22})_2]^{II}$. ^{1}H NMR (300 MHz, CD_3CN, p.p.m.): δ 8.790 (s, 4H, CH═N), 8.643–8.591 (t, 2H, H^a, J = 7.8 Hz), 8.308–8.282 (d, 4H, H^b, J = 7.8 Hz), 7.279–7.250 (d, 8H, H^d, J = 8.7 Hz), 6.752–6.722 (d, 8H, H^c, J = 9 Hz). MS (ESI): m/z (%): 386.2 (100) $[Zn(L_{22})_2]^{II}$. The ^{1}H NMR spectrum is displayed in Fig. S6.

2.3.3. Complex $[Zn(L_{33})_2]^{II}$. ^{1}H NMR (300 MHz, CD_3CN, p.p.m.): δ 8.809 (s, 4H, CH═N), 8.646–8.594 (t, 2H, H^a, J = 7.8 Hz), 8.321–8.295 (d, 4H, H^b, J = 7.8 Hz), 7.427–7.397 (d, 8H, H^d, J = 9 Hz), 6.691–6.661 (d, 8H, H^c, J = 9 Hz). MS (ESI): m/z (%): 476.2 (100) $[Zn(L_{33})_2]^{II}$. The ^{1}H NMR spectrum is displayed in Fig. S7.

2.3.4. Complex $[Zn(L_{44})_2]^{II}$. ^{1}H NMR (300 Hz, CD_3CN, p.p.m.): δ 8.800 (s, 4H, CH═N), 8.637–8.585 (t, 2H, H^a, J = 8.1, 7.5 Hz), 8.306–8.280 (d, 4H, H^b, J = 7.8 Hz), 7.616–7.587 (d, 8H, H^d, J = 8.7 Hz), 6.536–6.507 (d, 8H, H^c, J = 8.7 Hz). MS (ESI): m/z (%): 569.28 (100) $[Zn(L_{44})_2]^{II}$. The ^{1}H NMR spectrum is displayed in Fig. S8.

2.4. Single-crystal structures of $[Zn(L_{11})_2]^{II}$–$[Zn(L_{44})_2]^{II}$ complexes: data collection, structure solution and refinement

The diffraction intensities were collected at the joint X-ray Scattering Service of the Pôle Balard of the University of Montpellier II, France, at 175 K using an Agilent Technologies Xcalibur-I ($[Zn(L_{44})_2](CF_3SO_3)_2$) and a Gemini-S diffractometer ($[Zn(L_{11})_2](CF_3SO_3)_2$, $[Zn(L_{22})_2](CF_3SO_3)_2$, $[Zn(L_{33})_2](CF_3SO_3)_2$). The crystal-to-detector distance was 50 mm for the Xcalibur-I measurement, and 45 mm for the other three measurements. The structures were solved by *ab initio* (charge-flipping) methods using *SUPERFLIP* (Palatinus & Chapuis, 2007) and refined by least-squares methods on F using *CRYSTALS* (Betteridge *et al.*, 2003), against $|F|$ on data having $I > 2\sigma(I)$; R factors are based on these data. H atoms were partly located from difference-Fourier synthesis, partly placed based on geometrical arguments, and in general not refined. Non-H atoms were refined anisotropically. In the case of $[Zn(L_{11})_2](CF_3SO_3)_2$ a faint superstructure causing a doubled b axis was observed. The mean $\langle I/\sigma(I)\rangle$ values for hkl: h,k,l even and odd are 21.36 and 21.21 (h), 27.20 and 15.28 (k), 21.36 and 21.21 (l), respectively. Since the odd k reflections are far from extinct, it was decided that the b axis is truly doubled, and that the structure is commensurately modulated along this axis. Nine reflections were removed from this refinement because they were partly obscured by the beamstop shadow. The maximum positive electron density, 3.04 e Å^{-3}, is found at 0.797 Å from S158. In view of the presence of the main positive residual Fourier difference peaks close to trifluoromethanesulfonate atoms and the relatively large atomic displacement ellipsoids of the O and F atoms, it seems likely that most trifluoromethanesulfonate anions are partially orientationally disordered. No attempts were made to model this disorder. It appeared impossible to find untwinned or single fragment crystals of $[Zn(L_{22})_2](CF_3SO_3)_2$ and $[Zn(L_{33})_2](CF_3SO_3)_2$, which partly explains the relatively high R factors for these compounds. The data collection of $[Zn(L_{22})_2](CF_3SO_3)_2$ was carried out on a three-component specimen for which the second domain is rotated by 90° and the third domain by 180° around c^* of the first domain, which can be explained by the lattice metrics which are not very far from tetragonal. Fourteen beamstop-affected reflections were removed from the refinement. The highest positive difference electron density, 2.63 e Å^{-3}, was found at 0.972 Å from Zn1. $[Zn(L_{33})_2](CF_3SO_3)_2$ was found to be twinned by 180° rotation around the c^* axis. Ten beamstop affected reflections were removed from the least-squares calculation. A maximum difference electron density peak of 3.23 e Å^{-3} was found close to a phenyl ring at 1.21 Å from H211. The X-ray data of

[1] Supplementary data for this paper are available from the IUCr electronic archives (Reference: EB5021). Services for accessing these data are described at the back of the journal.

$[Zn(L_{44})_2](CF_3SO_3)_2$ were relatively weak; thermal similarity restraints [U(IJ) in *CRYSTALS* language] and also vibration restraints (VIBR) were applied to a number of C atoms in aromatic rings. A 'squeeze' correction was also applied (van der Sluis & Spek, 1990; Spek, 2003) to the structure factors in order to account for disordered electron density in a fairly large solvent accessible void, approximately 273 Å^3 and 126 electrons. Molecular structure diagrams with atom-labelling schemes can be found in Figs. S10–S13. Details concerning the data collection and structure refinement are compiled in Table S1. Full details can be found in the CIF files. All figures, except Fig. 1 which was made using *Mercury* (Macrae *et al.*, 2008) and Fig. 13 which was made with *Jmol* (Jmol, 2011), have been made with *OLEX2* (Dolomanov *et al.*, 2009).

3. Results and discussion

3.1. Structure similarity and crystal packing

All four crystal structures crystallize in the space group $P\bar{1}$, with two independent $[Zn(L_{ii})_2]^{II}$ moieties in the asymmetric part of the unit cell for $[Zn(L_{11})_2](CF_3SO_3)_2$ and one for the three others. At first sight, the unit-cell parameters (Niggli-reduced) reported in Table S1 suggest that the compounds are not isostructural or even closely related, with only some resemblance between the cell axis parameters of only $[Zn(L_{11})_2](CF_3SO_3)_2$, $[Zn(L_{22})_2](CF_3SO_3)_2$, and $[Zn(L_{33})_2](CF_3SO_3)_2$, but remarkable different angles.

In order to find an eventual structure similarity, structure packing calculations were carried out using the method proposed by Chisholm & Motherwell (2005) and implemented in the program *Mercury* 2.3 (Macrae *et al.*, 2008). A cluster of a maximum of 15 units surrounding the central moiety was defined and bonds and angles were assumed to be within the range of 'isostructurality' if they were within 20% for the bonds and within 20° for the angles, respectively. For the sake of simplicity the halogen atoms bound to the outermost phenyl rings of the two PDA-R moieties were withdrawn from the comparisons, since the C-Hal distance by itself already varies between 1.35 Å for C—F and 2.09 Å for C—I, a difference of 35% with respect to the longest one. In addition, calculations were carried out with and without the trifluoromethanesulfonate anions included. Table S2 summarizes some of the results. Two qualifiers were used for structure similarity, firstly a root-mean-square value based on the atomic coordinates within the specified tolerances and, secondly, the powder diffraction similarity index which was proposed elsewhere to be a measure for structure similarity (de Gelder *et al.*, 2001). A powder diagram was calculated for each structure and the powder similarity index was calculated for each pair. A value of 1 means that there is perfect agreement; the r.m.s. value should of course be the lowest possible for an optimal match between the crystal packing. Table S2 shows that the closest similarity for the central $[Zn(L_{ii})_2]^{II}$ moieties is found for Cl (i = 2) and Br (i = 3), but that the similarity is also very good with the two independent $[Zn(L_{11})_2]^{II}$ moieties. A notable difference between the crystal arrangement of $[Zn(L_{11})_2](CF_3SO_3)_2$ and $[Zn(L_{ii})_2](CF_3SO_3)_2$ (i = 2, 3) is the mass density which is slightly higher for the former than for the latter, contrary to what is expected from a perfect isostructurality. This is also expressed by the Kitajgorodskij packing indices (Kitajgorodskij,

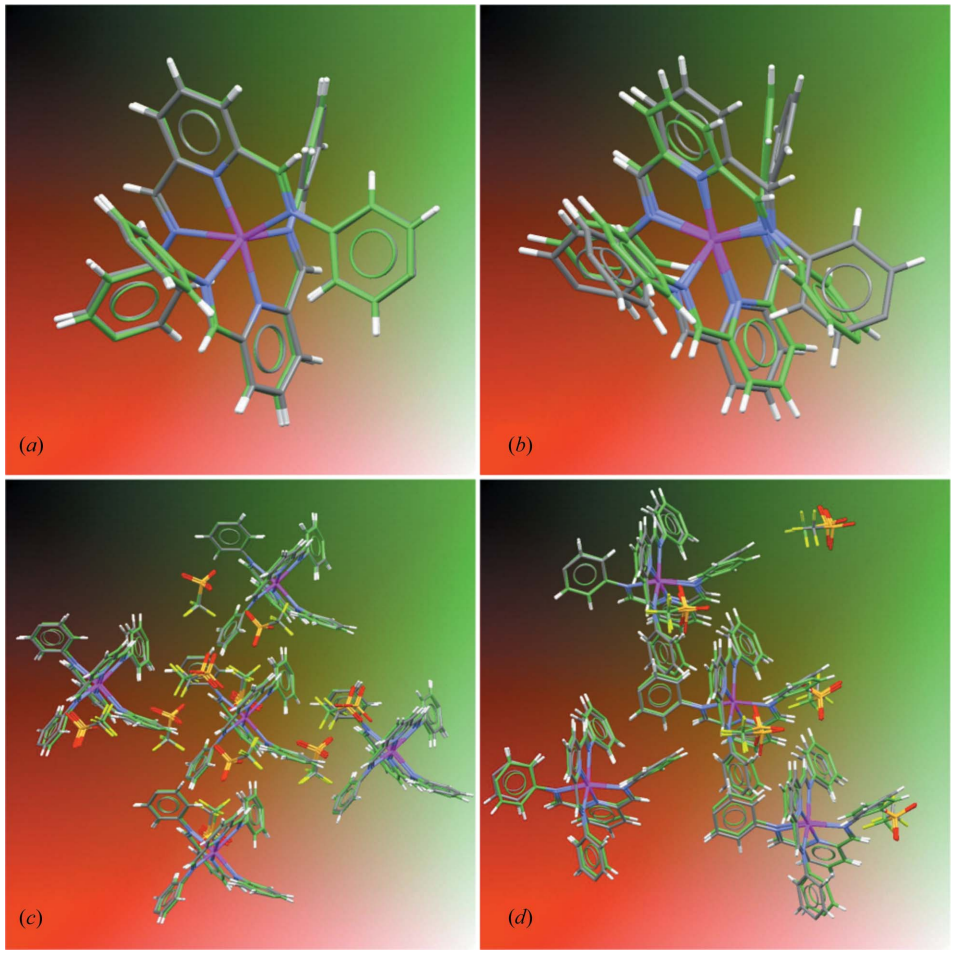

Figure 1
(*a*) Overlay of $[Zn(L_{ii})_2]^{II}$ moieties for $[Zn(L_{22})_2]^{II}$ and $[Zn(L_{33})_2]^{II}$; (*b*) overlay of $[Zn(L_{ii})_2]^{II}$ moieties for $[Zn(L_{33})_2]^{II}$ and $[Zn(L_{44})_2]^{II}$ moieties; (*c*) overlay of 15 units containing clusters for $[Zn(L_{22})_2]^{II}$ and $[Zn(L_{33})_2]^{II}$; (*d*) overlay of 9 units containing clusters for $[Zn(L_{11})_2]^{II}$ and $[Zn(L_{22})_2]^{II}$.

1973; Spek, 2003), which are 67.8, 65.1 and 64.1%, for the F, Cl and Br analogues, respectively.

On the other hand, the difference with the $[Zn(L_{44})_2]^{II}$ moiety is greater, which becomes immediately clear if the moieties are overlaid. In the latter case one phenyl moiety is in nearly perpendicular conformation with respect to the equivalent rings of the other halogen counterparts (Fig. 1*b*). This has important consequences for the crystal packing, which, according to Table S3, is only similar for the first three halogen analogues, but not any similarity is found with the I analogue. Fig. 1(*c*) shows the overlay of the Br and Cl analogues, which despite the cell-angle differences are strikingly similar.

The less-close similarity between the Cl and Br analogues on the one hand and the F analogue on the other hand is explained by the commensurate modulation along the *b* axis (see also §2). The apparent doubling of the *b* axis is illustrated in Fig. 2 where it can be seen that the two $[Zn(L_{ii})_2]^{II}$ moieties of the lower half are repeated in the upper half of the unit cell. It is noted that the two crystallographically independent $[Zn(L_{ii})_2]^{II}$ moieties of the upper half are also related by an inversion centre to those of the lower half. The same is true for the crystallographically independent trifluoromethanesulfonate counterions T2 and T4, *i.e.* **r**(T4_UH) = 1 − **r**(T4_LH) ≃ **r**(T2_LH) + **b**/2, where UH denotes the 'upper half' and LH 'lower half'. However, this is not true for trifluoromethanesulfonates T1 and T3, where only the centre of gravity of T1 and T3 approximately fulfils the relation **r**(T3_UH) = 1 − **r**(T3_LH) ≃ **r**(T1_LH) + **b**/2, but not the individual constituents of the anion: the two anions appear to be rotated by approximately 90° around a line parallel to the *c* axis.

3.2. General packing features

The packing of the structures of $[Zn(L_{ii})_2](CF_3SO_3)_2$ (*i* = 1, 2, 3) is dominated by $[Zn(L_{ii})_2]^{II}$ moieties which are stacked both along the *a* axis and the *b* axis. The $[Zn(L_{ii})_2]^{II}$ moieties are mutually interconnected by trifluoromethanesulfonate counterions in the space between the columns, as is shown in Fig. 3. The packing of $[Zn(L_{44})_2](CF_3SO_3)_2$ differs from that of the others, because no single $[Zn(L_{ii})_2]^{II}$ columnar stacks are formed but instead double $[Zn(L_{ii})_2]$ columnar stacks propa-

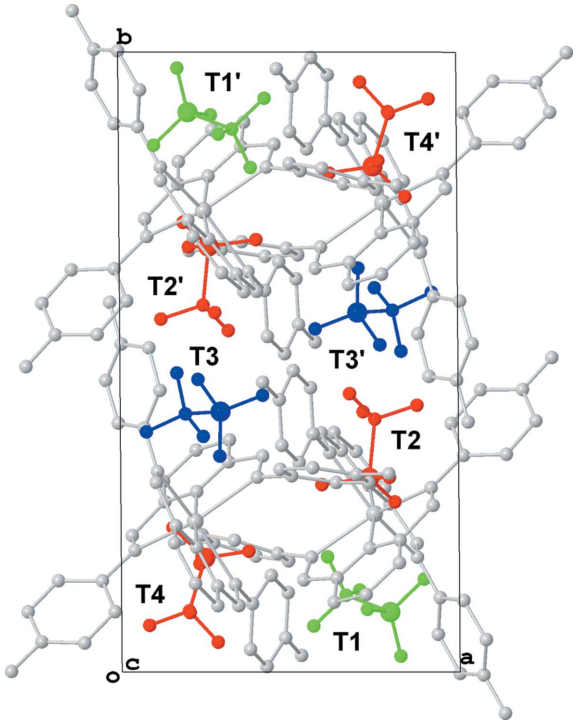

Figure 2
Projection along the *c* axis of the structure of $[Zn(L_{11})_2](CF_3SO_3)_2$. H atoms have been omitted for clarity. Zn and PDA-*R* ligands are in light grey and trifluoromethanesulfonate counterions are in red, green and blue.

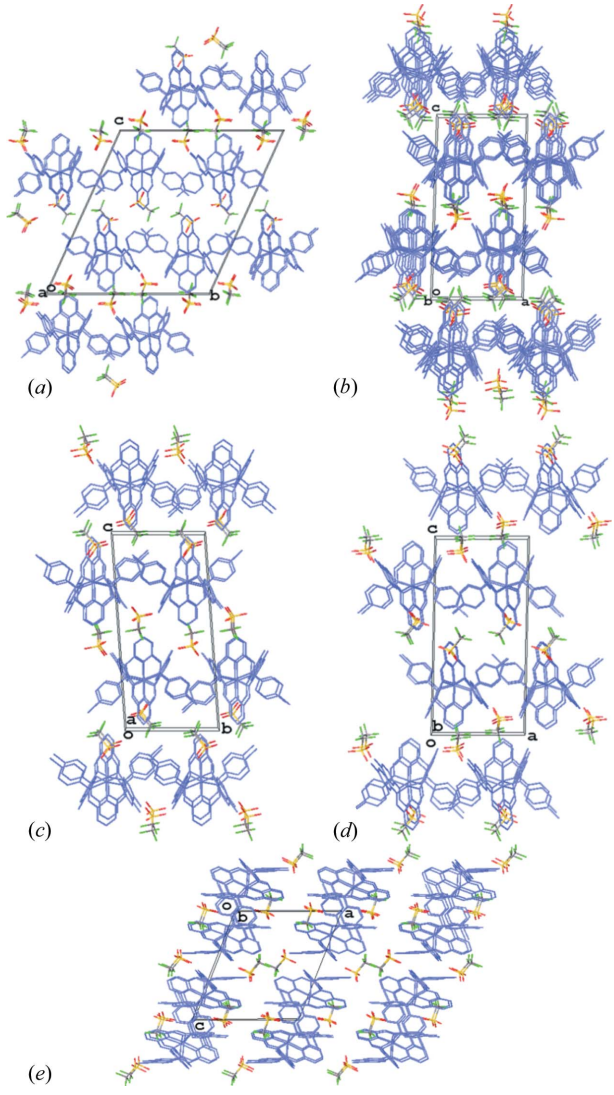

Figure 3
Packing of $[Zn(L_{ii})_2]^{II}$ moieties along the *a* and *b* axes. (*a*)–(*b*) $[Zn(L_{11})_2](CF_3SO_3)_2$; (*c*)–(*d*) $[Zn(L_{22})_2](CF_3SO_3)_2$; (*e*) $[Zn(L_{44})_2](CF_3SO_3)_2$. H atoms have been omitted for clarity. All figures have been drawn with a slight perspective view.

gating in only one direction. Fig. 3 also shows that the structures may be considered as being built up by alternating cationic $[Zn(L_{ii})_2]^{2+}$ sheets and double anionic layered $(CF_3SO_3)_2^{2-}$ sheets, which are stacked along the *c* direction. Fig. 4 compares the columnar stacks for $[Zn(L_{ii})_2](CF_3SO_3)_2$ (i = 1, 2, 3) with that for $[Zn(L_{44})_2](CF_3SO_3)_2$. It may appear from the figure that the $[Zn(L_{33})_2]^{II}$ stacks are connected by weak $\pi\cdots\pi$ interactions, but this is not the case since the closest distances between aromatic centroids are 4.33 (1) and 4.830 (9) Å, respectively, much larger than the distance (4.0 Å) beyond which an attractive interaction may exist.

Another difference between the structures of $[Zn(L_{ii})_2](CF_3SO_3)_2$ (i = F, Cl, Br) on the one hand and that of the iodo analogue on the other hand is the presence of solvent accessible voids in the latter (see also §2). The voids are aligned in channels running along the *c* axis and are actually filled with highly disordered solvent molecules (Fig. 5).

The very close isostructurality of the structures of $[Zn(L_{ii})_2](CF_3SO_3)_2$ (i = 1–3) becomes clear when the packing of the cationic $[Zn(L_{ii})_2]^{II}$ units and the anionic $CF_3SO_3^-$ trifluoromethanesulfonate moieties is considered. Fig. 6 gives the anionic surrounding of the $[Zn(L_{ii})_2]^{II}$ units within 2.5 Å: only one trifluoromethanesulfonate anion out of four independent ones in the structure of $[Zn(L_{11})_2](CF_3SO_3)_2$ has a different orientation with respect to the equivalent independent trifluoromethanesulfonate anion in $[Zn(L_{22})_2](CF_3SO_3)_2$ and $[Zn(L_{33})_2](CF_3SO_3)_2$. All other trifluoromethanesulfonate anions have approximately the same orientation with respect to the $[Zn(L_{ii})_2]^{II}$ units.

3.3. Weak interactions involving halogen atoms and other non-classical interactions involving hydrogen and/or π systems

It is generally accepted that hydrogen bonds involving halogen atoms, halogen bonding and halogen–halogen interactions may play an important role next to 'classical' hydrogen bonding in supramolecular chemistry (Brammer *et al.*, 2001; Csöregh *et al.*, 2001; Ouvrard *et al.*, 2003; Awwadi *et al.*, 2006). In the case of hydrogen bonds involving halogen atoms the halogens act as hydrogen-bond acceptors and would involve for the present four structures trifluoromethanesulfonate fluorine – hydrogen bonded to PDA-*R* moieties or terminal Ph-halogens hydrogen bonded to other PDA-*R* moieties. Covalently bound fluorine is generally believed not to act as a hydrogen-bond acceptor (Dunitz & Taylor, 1997), with OH and NH as hydrogen-bond donors, thus it will be even less likely with CH as a donor, although exceptions may of course occur. For the sake of completeness, and because of the isostructurality of the F, Cl and Br analogues, we list possible interactions for all analogues.

In the case of halogen bonding, it is the halogen atom which acts as the electrophilic species and replaces the role of the proton in hydrogen bonding. In the present structures this involves interactions between terminal Ph-Hal atoms and trifluoromethanesulfonate O atoms. In contrast with hydrogen bonding involving halogen atoms, it is naturally fluorine which has the weakest interaction. Several studies have been devoted to the question whether C—F$\cdots A$ (*A*: a fluorine bond acceptor) interactions actually exist or not, in view of their

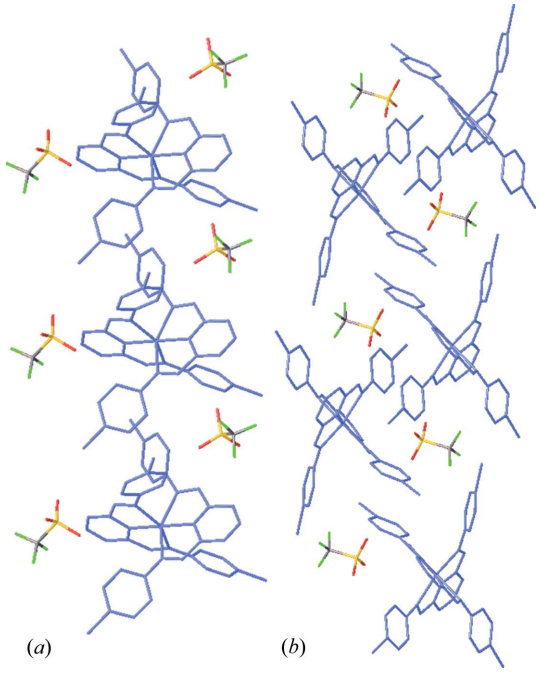

Figure 4
$[Zn(L_{ii})_2]^{II}$ stacks propagating along the *b* axis. (*a*) $[Zn(L_{ii})_2]^{II}$ single stacks; (*b*): $[Zn(L_{ii})_2]^{II}$ double stacks.

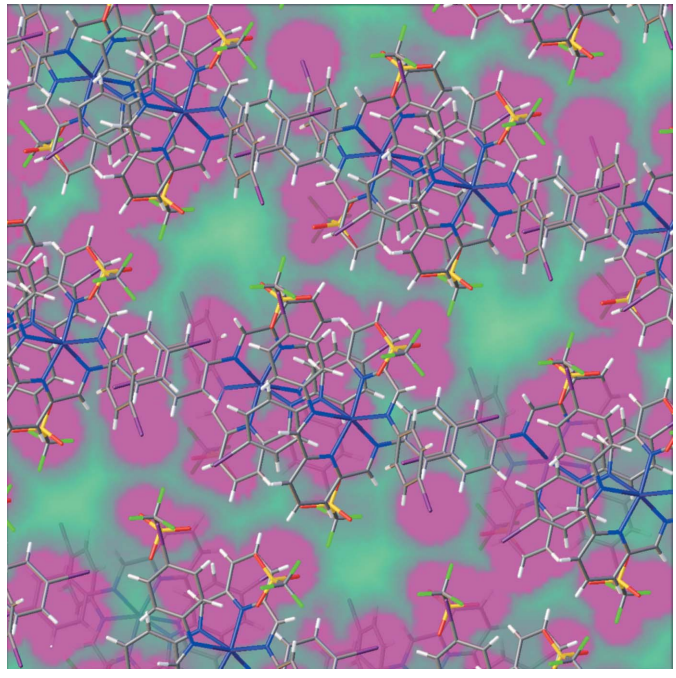

Figure 5
Solvent-accessible channels running along the *c* axis in the structure of $[Zn(L_{44})_2](CF_3SO_3)_2$. Areas of low electron density are in green, whereas areas of high electron density are in purple.

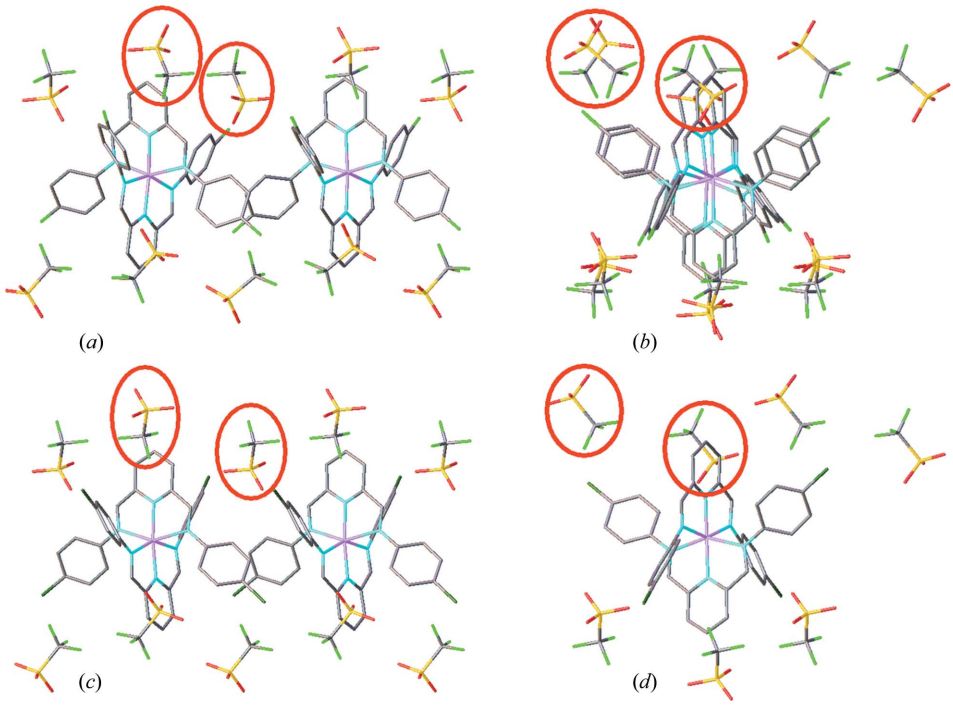

Figure 6
Anionic surrounding of the $[Zn(L_{ii})_2]^{II}$ units in the structure of $[Zn(L_{22})_2](CF_3SO_3)_2$ (*a*)–(*b*) and the structure of $[Zn(L_{22})_2](CF_3SO_3)_2$ (*c*)–(*d*). Projections along the *b* axis for (*b*) and (*c*) and along the *a* axis for (*a*) and (*d*). Trifluoromethanesulfonate anions in the two red circles of (*a*)–(*b*) are related by an inversion center.

exceptional weakness (Chopra & Guru Row, 2008; Ojala *et al.*, 2010). Very recently, however, evidence has been presented for the possible halogen-bond donor character of fluorine by a combined experimental and theoretical study (Dikundwar & Guru Row, 2012).

Halogen–halogen interactions are finally understood as the result of electrostatic attractive forces due to the presence of a positive electrostatic end cap on the halogen and the anisotropically distributed electron density around the halogen atom.

It is interesting to note that 'classical' hydrogen bonds such as OH···N or OH···O are not present in any of the four halogen analogues, thus it must be assumed that the three before-mentioned weak interactions involving halogen atoms are responsible for the structural cohesion, besides possible π–π or CH···π and CHal···π interactions as well as CH···O interactions. The latter interactions have been investigated recently for aromatic CH groups and different types of O acceptors (Veljković *et al.*, 2011): it was shown that there is only a slight preference for linear contacts, depending mainly whether the interaction is bifurcated or not. Interaction energies are in general slightly lower than -4.19 kJ mol^{-1}.

Since the first three structures are essentially isostructural, it is interesting to see if these and other interactions may play a role in the supramolecular packing of these compounds. Isostructurality usually implies that the intermolecular interactions are relatively similar, thus the investigation of the interactions in $[Zn(L_{ii})_2](CF_3SO_3)_2$ may reveal the relative weights of each of the contributions. Normally, isostructurality never extends over all four Hal analogues of a particular (organic) compound (Grineva & Zorkii, 2001; Saha & Nangia, 2007); Br and Cl substituents are most frequently isostructural, and the chloro/bromo/iodo isostructurality is encountered in *ca* 30% of the pre-cited series.

Tables S4–S7 summarize intermolecular distances between halogen or H atoms and F and O atoms of the trifluoromethanesulfonate counterions whenever the normalized distance $d_{norm} = d/(r_1 + r_2) < 1.10$, where r_1 and r_2 are the van der Waal's radii of the constituents. The van der Waal's radii were taken from Bondi (1964): F 1.47, Cl 1.75, Br 1.85, I 1.98, O 1.52, H 1.20 Å. As was pointed out by Dunitz & Taylor (1997), any distance limit under which an interaction could be considered as halogen or hydrogen bonding is arbitrary. We have chosen a rather soft limit $d_{norm} < 1.10$ in line with other authors (Jeffrey & Saenger, 1991). Table S8 gives distances and angles for CH···π interactions. In this study the C—H distances were not normalized to their neutron values of 1.08 Å.

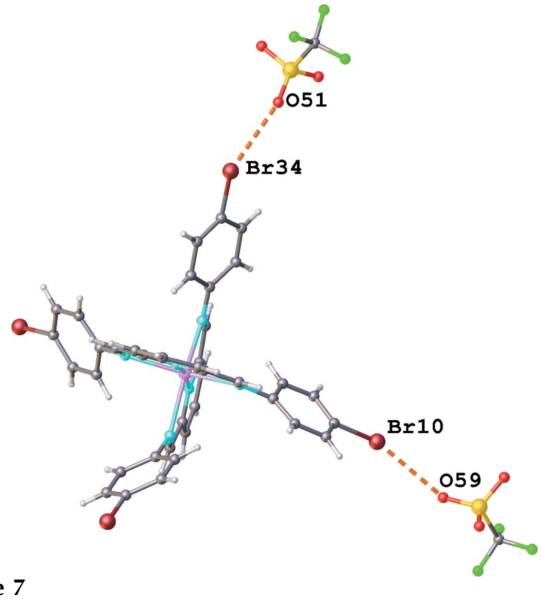

Figure 7
$[Zn(L_{33})_2](CF_3SO_3)_2$ complex showing Br···O halogen bonds.

3.4. Weak interactions involving oxygen as the halogen bond acceptor

Table S6 shows that C—Hal···O bonds are apparently present for $[Zn(L_{ii})_2]^{II}$ (i = 2–4) analogues having d_{norm} values equal or lower than 1.00 and close to 180° C—Hal···O angles. This quasi-linearity of the contact angle is a clear signature of the existence of the bond, and is even more pronounced than for hydrogen bonds (Ouvrard *et al.*, 2003). In $[Zn(L_{22})_2]^{II}$ and $[Zn(L_{33})_2]^{II}$ there are two of these bonds, one on each PDA-Br arm. In this way $[Zn(L_{33})_2](CF_3SO_3)_2$ isolated trimers are formed, as shown in Fig. 7 for $[Zn(L_{33})_2]^{II}$. There is thus not an infinite network connecting all moieties. In the I analogue, only one I···O bond is found, but most probably the second arm is bonded to the disordered solvent water molecules present in the voids of the structure. Interestingly, the F analogue is shown not to form F···O bonds, although it is isostructural to $[Zn(L_{ii})_2](CF_3SO_3)_2$ (i = 2, 3). This is not surprising in view of the fact that chlorine and bromine are more electrophilic than fluorine, so it can in fact be questioned whether the apparent Cl···O and Br···O interactions play a very important role in stabilizing the crystal structure packing.

3.5. Weak interactions involving halogen as a hydrogen bond acceptor

Similarly, possible C—H···Hal interactions can be investigated for their role in the structural cohesion. The van der Waals radius of H is very often taken to be 1.20 Å (Bondi, 1964), but is sometimes taken to be 1.09 Å). In view of this incertitude and also of the incertitude in the crystallographic position of the proton, intermolecular H···Hal distances below 2.93, 3.24, 3.35 and 3.49 Å for $[Zn(L_{ii})_2](CF_3SO_3)_2$ (i = 1–4), respectively, were considered to be potentially bonding (Table S4). Interestingly, the C—H···Hal interaction which seems to give one-dimensional cohesion in $[Zn(L_{ii})_2](CF_3SO_3)_2$ [i = 2, 3; distances 2.793 (5) and 2.882 (6) Å for the Cl and Br analogue, respectively; Fig. 8] is absent in $[Zn(L_{44})_2](CF_3SO_3)_2$: the corresponding shortest distance is 2.992 Å.

Other CH···F distances between 2.53 and 2.80 Å almost fulfill the criterion of 'interacting' (Chopra & Guru Row, 2005), but they are in general not very directional, with CH···F angles in general smaller than 140°. This shows again that attracting CH···Hal interactions are unlikely to be responsible for the crystal packing in these compounds.

3.6. Weak interactions involving the halogen as a halogen-bond acceptor and donor

In this section halogen–halogen interactions are investigated for their role in crystal packing. In this particular case these interactions concern those between F atoms of the trifluoromethanesulfonate moieties and halogen atoms of the PDA-*R* moieties. The iodine analogue does not show any interaction between the PDA-*R* iodine and the trifluoromethanesulfonate F atoms. However, as shown in Table S5, it appears that in the three other cases CF···Hal angles cluster around 90 and 180°, with $0.98 < d_{norm} < 1.10$. Halogen–halogen interactions are usually divided into two types, type I and type II, where type I interactions have C—Hal1···Hal2 and Hal1···Hal2—C angles approximately equal – either in a *cis* or a *trans* geometry – and type II interactions where the first angle is approximately 90° and the second one approximately 180° (Ramasubbu *et al.*, 1986). Type I interactions are predominant for homo-halogen interactions, whereas type II interactions prevail for hetero-halogen interactions. Interestingly, for $[Zn(L_{ii})_2](CF_3SO_3)_2$ (i = 1–3), type I interactions seem to be dominant, thus both for homo-halogen (F—F) as well as for hetero-halogen interactions (F—Cl and F—Br). Fig. 9 shows the potential interactions of the double-arm PDA-*R* moiety with surrounding trifluoromethanesulfonate counterions for the two independent PDA-F complexes and the PDA-Cl moiety, respectively. An important difference is that the the PDA-Cl (and also PDA-Br) peripheral atoms have per arm one linear and one perpendicular halogen–halogen contact with a fluorine atom from a trifluoromethanesulfonate counterion, whereas the two PDA-F moieties have only one linear contact and three perpendicular contacts per moiety. This suggests that the isostructurality between the fluorine analogue on the one hand and the chlorine and bromine analogues on the other hand is indeed less perfect than that between the chlorine and bromine analogues, as could already

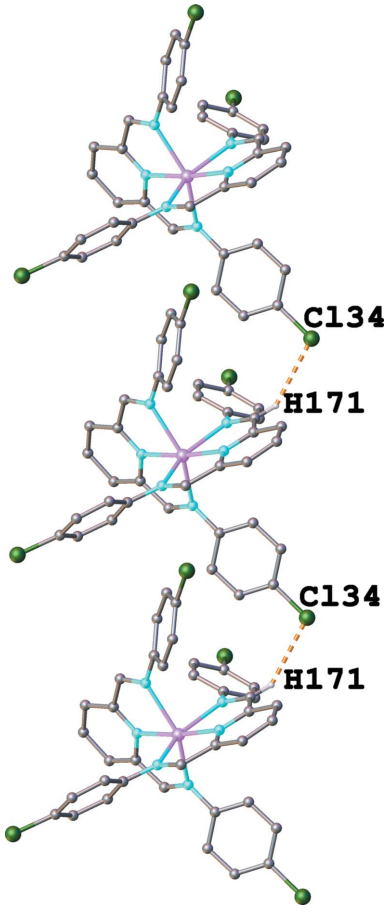

Figure 8
$[Zn(L_{22})_2](CF_3SO_3)_2$ complex showing one-dimensional chains formed by CH···Cl interactions.

be anticipated from the overlay calculations in *Mercury* where a good fit was only obtained for 9 units, instead of at least 15 units between the bromine and chlorine analogues (Fig. 2). The principal reason is that some of the trifluoromethanesulfonate counterions in the structure of $[Zn(L_{11})_2](CF_3SO_3)_2$ have a different orientation than those in $[Zn(L_{22})_2](CF_3SO_3)_2$ and $[Zn(L_{33})_2](CF_3SO_3)_2$. The trifluoromethanesulfonate counterions appear therefore to play a subtle role in the crystal packing of these compounds.

3.7. Weak interactions involving π-systems

Apart from the role of the trifluoromethanesulfonate counterions in the cohesion of the crystal packing $\pi\cdots\pi$ or CH$\cdots\pi$ interactions between PDA-*R* moieties could equally well give additional stability to the crystal structure. This occurs for instance in the homochiral double-helical Zn^{II}-, Co^{II}- and Fe^{II}-PDA complexes (Dumitru *et al.*, 2009). However, in the present four analogues no Cg–Cg (where Cg is the centroid of an aromatic ring) are found implying that $\pi\cdots\pi$ interactions are absent. A limited number of weak aromatic intermolecular Cg—H (Table S7) interactions are, however, found in all four structures with Cg$\cdots$H distances below 3.0 Å. Fig. 10 shows that they all concern H atoms which are at a terminal phenyl ring next to the halogen atom. No direct evidence is found for C—Hal$\cdots\pi$ interactions.

3.8. Weak CH$\cdots$O interactions

Weak CH$\cdots$O interactions below 2.72 Å are listed in Table S7; in comparison with the interactions involving halogen they appear to be more directional and also stronger with respect to d_{norm} for which values lower than 0.9 are found for $[Zn(L_{11})_2](CF_3SO_3)_2$ and the $[Zn(L_{22})_2](CF_3SO_3)_2$ complexes. The d_{norm} values for $[Zn(L_{ii})_2](CF_3SO_3)_2$ (i = 2, 3) are in general slightly higher. Fig. 11 shows the CH$\cdots$O interactions for the F and Cl interactions where only the independent trifluoromethanesulfonate anions (4 for the F analogue and 2 for the Cl analogue) are shown. CH$\cdots$O interactions bind in the structure of $[Zn(L_{22})_2](CF_3SO_3)_2$ trifluoromethanesulfonate anions to PDA-*R* moieties in only one cationic sheet. The same is true for three of the four independent trifluoromethanesulfonate anions in the structure of $[Zn(L_{11})_2](CF_3SO_3)_2$; the fourth trifluoromethanesulfonate anion (depicted in a red circle in Fig. 11) binds thanks to its canted orientation with respect to the corresponding trifluoromethanesulfonate anion in $[Zn(L_{22})_2](CF_3SO_3)_2$ *via* an CH$\cdots$O interaction to a second cationic sheet, whereas a bifurcated CH$\cdots$O interaction exists to the first cationic sheet. The interaction of this trifluoromethanesulfonate anion with two cationic sheets *via* weak CH$\cdots$O interactions is the reason why there is no strict isostructurality between $[Zn(L_{11})_2](CF_3SO_3)_2$ on the one hand and $[Zn(L_{ii})_2](CF_3SO_3)_2$ (i = 2, 3) on the other hand.

Fig. 12 depicts the role of C—H$\cdots$O interactions in the structure of $[Zn(L_{44})_2](CF_3SO_3)_2$; here they couple the PDA-I blocks within and between the bicolumnar stacks by bi- or trifurcated interactions. The interactions are mostly highly directional and rather short, the shortest being only 2.364 (17) Å, *i.e.* 0.38 Å

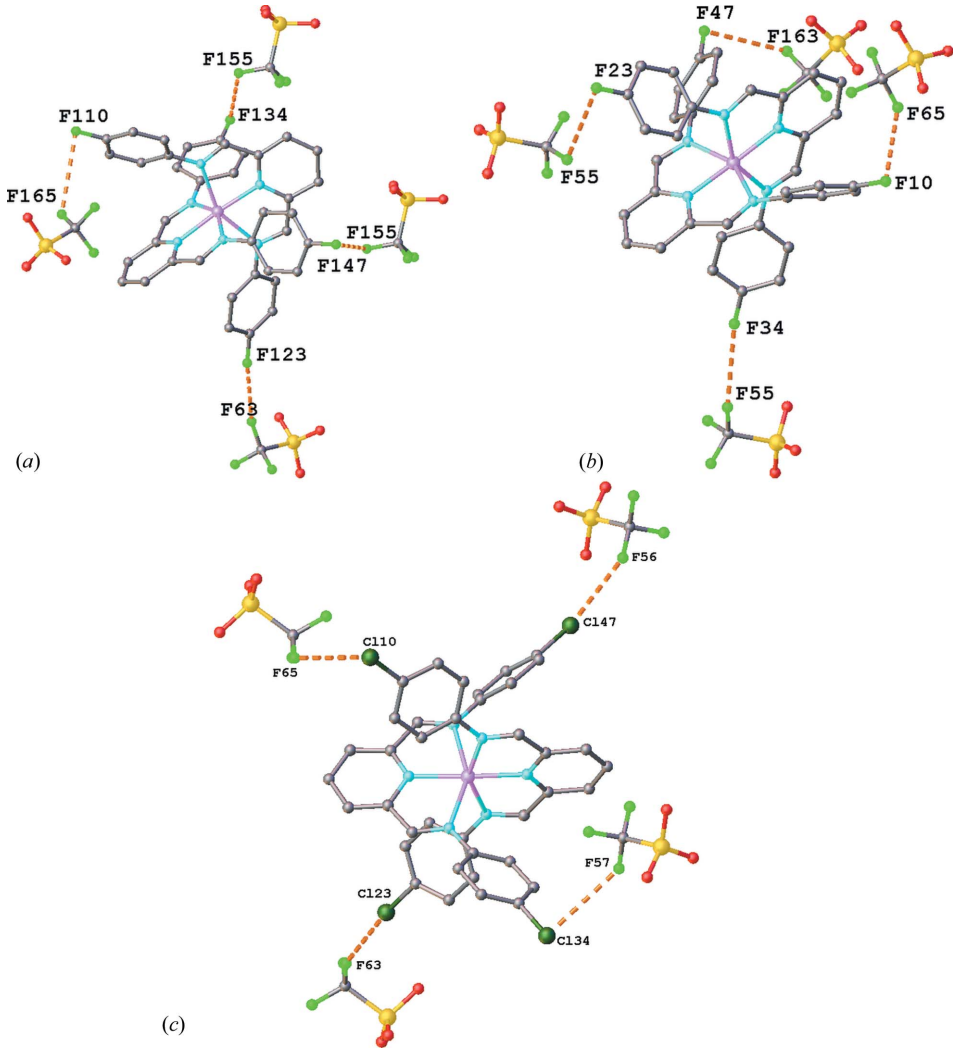

Figure 9
(*a*)–(*b*) CF$\cdots$FC interactions in the two independent $[Zn(L_{11})_2](CF_3SO_3)_2$ complexes. (*c*) CF$\cdots$ClC interactions in the $[Zn(L_{22})_2](CF_3SO_3)_2$ complex.

shorter than the sum of the van der Waal's radii of oxygen and hydrogen.

3.9. Calculation and visualization of non-covalent interactions based on the electron density and its derivatives

Non-covalent interactions cannot only be determined by an analysis of close contacts within the limit of the sum of the van der Waals radii of the constituents of the contacts, but also by a calculation of the electron density and its derivatives (Johnson *et al.*, 2010; Contreras-García *et al.*, 2011). The method is based on the fact that the critical points of the gradient of the electron density occur whenever atoms interact. This approach is not only capable of identifying the non-covalent interaction volumes, but also to quantify their relative strengths. We used here the implementation in *Jmol* for a qualitative analysis (Jmol, 2011). The *Jmol* implementation uses promolecular densities calculated from the atomic coordinates for the calculation of the reduced density gradient. Fig. 13 shows the contact areas in the structure of $[Zn(L_{22})_2](CF_3SO_3)_2$. The supplementary material contains a rotatable and zoomable model which makes it easier to spot the interaction areas (Fig. S14). The calculated interaction areas confirm largely the conclusions from the analysis of the contact distances. The strongest interactions which spread over the largest volume occur between the O atoms of the trifluoromethanesulfonate sulfonate groups and a number of H atoms of the PDA-Cl moieties (indicated by '1' in Fig. 13), whereas smaller interaction zones occur between terminal chloride atoms (indicated by '2') and H atoms of the central phenyl moiety of a PDA arm. Even smaller interactions exist between trifluoromethanesulfonate F atoms and PDA moieties.

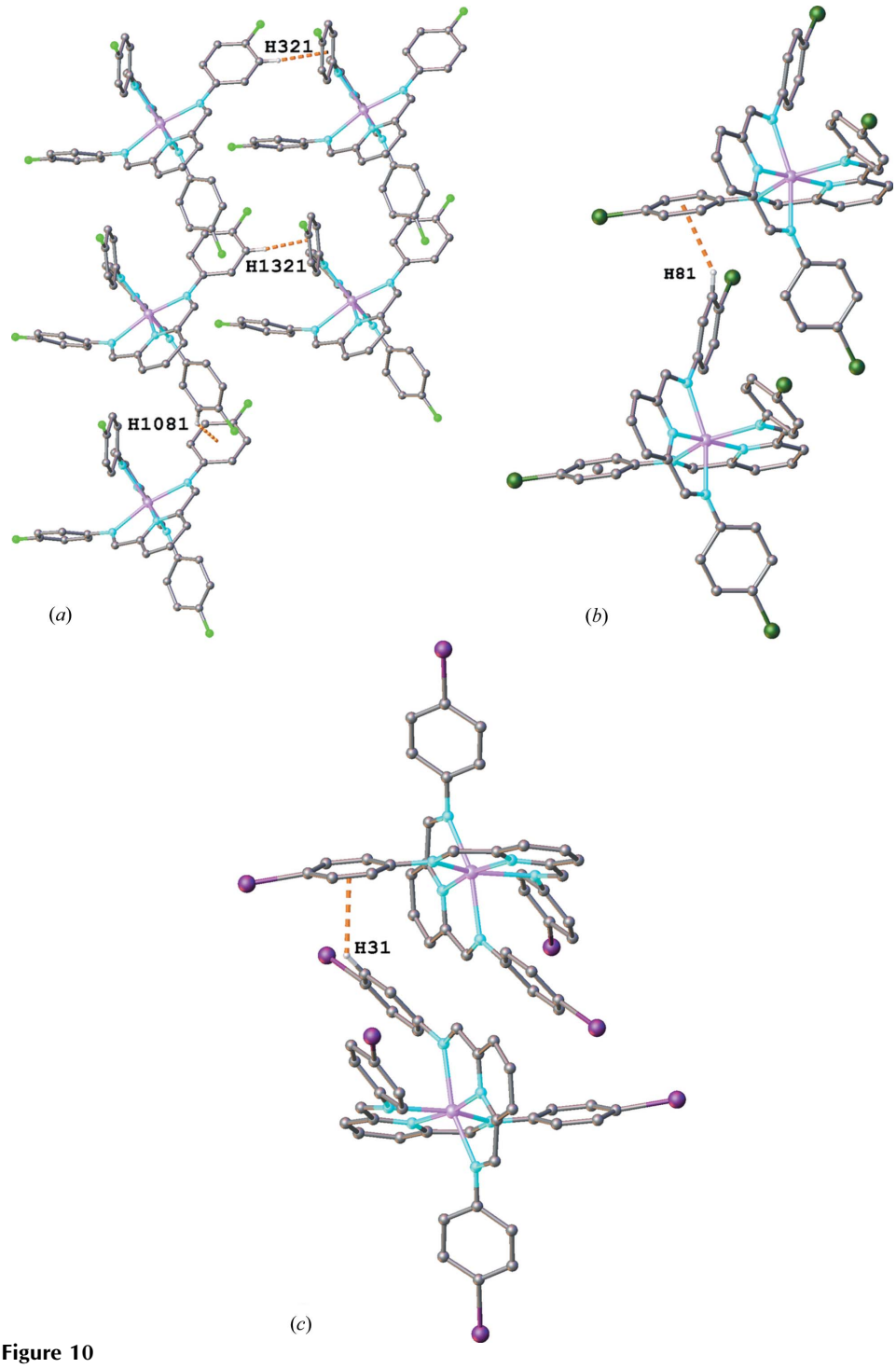

Figure 10
C—H···π interactions in (*a*) $[Zn(L_{11})_2](CF_3SO_3)_2$ and (*b*) $[Zn(L_{22})_2](CF_3SO_3)_2$. (*c*) C—H···$\pi$ interactions in the $[Zn(L_{44})_2](CF_3SO_3)_2$ complex.

4. Conclusions

The binding features and structural properties of an isomorphous series of halogen pseudoterpyridine Zn^{II} complexes involving weak interactions involving halogen atoms are discussed in this work, and its implications for the overall packing of $[Zn(L_{ii})_2]^{II}$ metallosupramolecular complexes that only differ in the nature of the aromatic halogen. Crystal packing is a complex interplay of competing interactions, including in this

particular case ionic, hydrogen and halogen bonding as well as π-stacking and van der Waal's interactions. At first sight, it seems that only H—Hal bonds will vary, with or without a direct impact on the packing, but the reality is more complex than this simplistic presumption. Although isostructurality of halogen analogues is far from being common, in this study the Cl and Br analogues are isostructural and the F analogue partly isostructural. Despite its close isostructurality, the F analogue is shown not to form Hal···O bonds, whereas the Cl and Br compounds do. Similarly, while the CH···Hal interaction seems to give one-dimensional cohesion in the Cl and Br analogues, this feature is absent in the F analogue. The major attractive interactions seem to come from CH···O interactions, which play a particular role in the F analogue, where halogen interactions are perhaps weaker than in the Cl and Br analogues. The constitutional self-organization into metallosupramolecular architectures around a metal-ion center is not related to metal *inner* coordination geometry but *outer* supramolecular/constitutional requirements are expressed differently as time as the role of Hal···O and CH···O interactions in the structuration of the crystal packing, particularly expressed in fine stabilization effects.

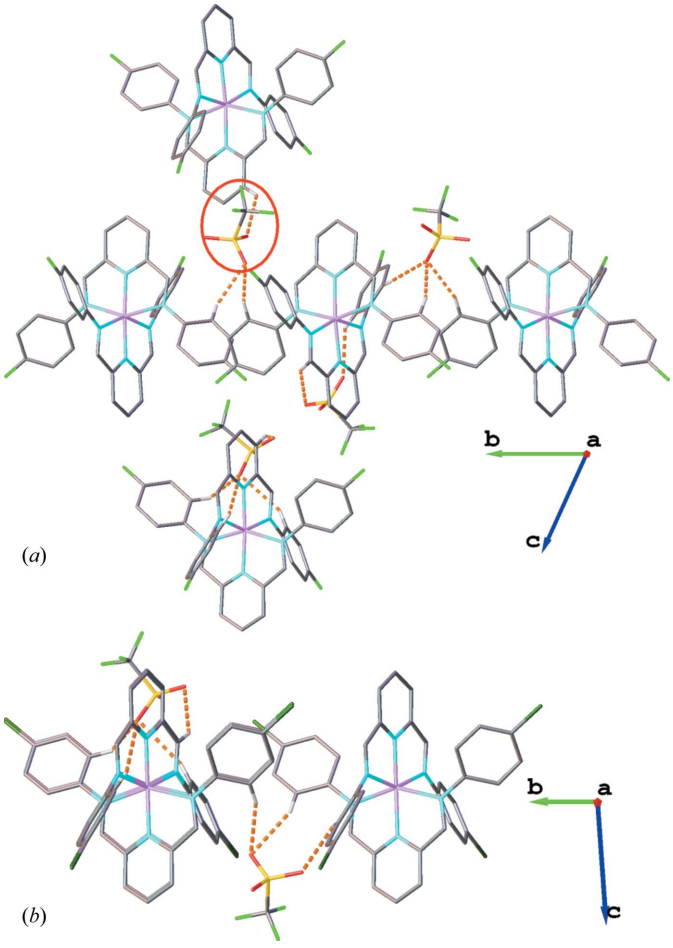

Figure 11
CH···O interactions in (*a*) $[Zn(L_{11})_2](CF_3SO_3)_2$ and (*b*) $[Zn(L_{22})_2](CF_3SO_3)_2$. Only H atoms involved in C—H···O interactions are drawn for the sake of clarity. The red circle denotes the same trifluoromethanesulfonate anion as in Fig. 6.

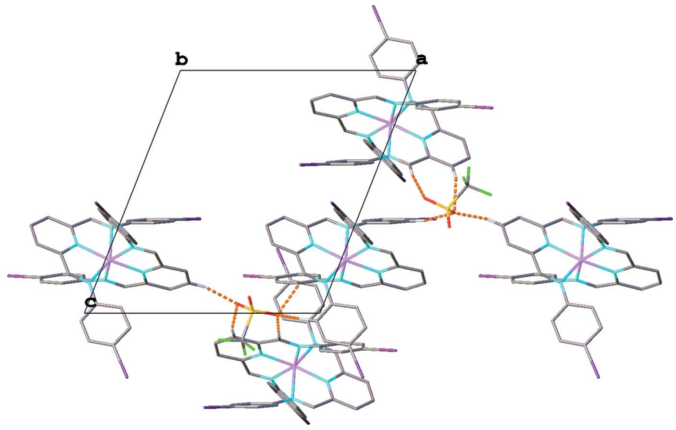

Figure 12
CH···O interactions in $[Zn(L_{44})_2](CF_3SO_3)_2$.

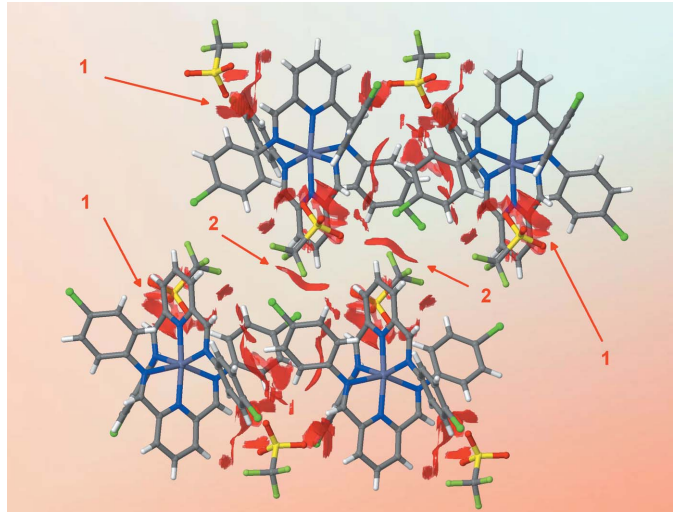

Figure 13
Non-covalent interaction zone (translucent red) between the different moieties in the structure of $[Zn(L_{22})_2](CF_3SO_3)_2$. The numbers refer to different areas explained in the text.

This work was conducted as a part of a DYNANO, PITN-GA-2011-289033 project. See www.dynano.eu.

References

Awwadi, F. F., Willet, R. D., Peterson, K. A. & Twamley, B. (2006). *Chem. Eur. J.* **12**, 8952–8960.
Barboiu, M. (2010). *Chem. Commun.* **46**, 7466–7476.
Barboiu, M. (2012). *Top. Curr. Chem.* **322**, 33–53.
Barboiu, M., Dumitru, F., Legrand, Y.-M., Petit, E. & van der Lee, A. (2009). *Chem. Commun.* **16**, 2192–2194.
Barboiu, M., Petit, E., van der Lee, A. & Vaughan, G. (2006). *Inorg. Chem.* **45**, 484–486.
Barboiu, M., Ruben, M., Blasen, G., Kyritsakas, N., Chacko, E., Dutta, M., Radekovich, O., Lenton, K., Brook, D. J. R. & Lehn, J.-M. (2006). *Eur. J. Inorg. Chem.* pp. 784–789.
Betteridge, P. W., Carruthers, J. R., Cooper, R. I., Prout, K. & Watkin, D. J. (2003). *J. Appl. Cryst.* **36**, 1487.
Bondi, A. (1964). *J. Phys. Chem.* **68**, 441–451.

Brady, P. A. & Sanders, J. K. M. (1997). *J. Chem. Soc. Perkin Trans. 1*, pp. 3237–3253.
Brammer, L., Bruton, E. A. & Sherwood, P. (2001). *Cryst. Growth Des.* **1**, 277–290.
Bruckmann, A., Pena, M. A. & Bolm, C. (2008). *Synlett*, **6**, 900–902.
Cariati, E., Forni, A., Biella, S., Metrangolo, P., Meyer, F., Resnati, G., Righetto, S., Tordin, E. & Ugo, R. (2007). *Chem. Commun.* **25**, 2590–2592.
Cavallo, G., Metrangolo, P., Pilati, T., Resnati, G., Sansotera, M. & Terraneo, G. (2010). *Chem. Soc. Rev.* **39**, 3772–3783.
Chisholm, J. A. & Motherwell, S. (2005). *J. Appl. Cryst.* **38**, 228–231.
Chopra, D. & Guru Row, T. N. (2005). *Cryst. Growth Des.* **5**, 1679–1681.
Chopra, D. & Guru Row, T. N. (2008). *CrystEngComm*, **10**, 54–67.
Choudhary, S. & Morrow, J. R. (2002). *Angew. Chem. Int. Ed.* **41**, 4096–4098.
Contreras-García, J., Johnson, E. R., Keinan, S., Chaudret, R., Piquemal, J., Beratan, D. N. & Yang, W. (2011). *J. Chem. Theory Comput.* **7**, 625–632.
Csöregh, I., Brehmer, T., Bombicz, P. & Weber, E. (2001). *Cryst. Eng.* **4**, 343–357.
Dikundwar, A. G. & Row, T. N. G. (2012). *Cryst. Growth Des.* **12**, 1713–1716.
Dolomanov, O. V., Bourhis, L. J., Gildea, R. J., Howard, J. A. K. & Puschmann, H. (2009). *J. Appl. Cryst.* **42**, 339–341.
Dumitru, F., Legrand, Y. M., van der Lee, A. & Barboiu, M. (2009). *Chem. Commun.* **19**, 2667–2669.
Dumitru, F., Petit, E., van der Lee, A. & Barboiu, M. (2005). *Eur. J. Inorg. Chem.* pp. 4255–4262.
Dunitz, J. D. & Taylor, R. (1997). *Chem. Eur. J.* **3**, 89–98.
Fourmigué, M. (2008). *Struct. Bond.* **126**, 181–207.
Fourmigué, M. & Batail, P. (2004). *Chem. Rev.* **104**, 5379–5418.
Gelder, R. de, Wehrens, R. & Hageman, J. A. (2001). *J. Comput. Chem.* **22**, 273–289.
Gonnade, R. G., Shashidhar, M. S. & Bhadbhade, M. M. (2007). *J. Indian Inst. Sci.* **87**, 149–166.
Goral, V., Nelen, M. I., Eliseev, A. V. & Lehn, J. M. (2001). *Proc. Natl Acad. Sci. USA*, **98**, 1347–1352.
Grineva, O. V. & Zorkii, P. M. (2001). *J. Struct. Chem.* **42**, 16–23.
Jeffrey, G. A. & Saenger, W. (1991). *Hydrogen Bonding in Biological Structures*, pp. 29–33. Berlin: Springer.
Jmol (2011). *Jmol: an open-source Java viewer for chemical structures in 3D*. http://www.jmol.org/.
Johnson, E. R., Keinan, S., Mori-Sánchez, P., Contreras-García, J., Cohen, A. J. & Yang, W. (2010). *J. Am. Chem. Soc.* **132**, 6498–6506.
Kitajgorodskij, A. I. (1973). *Molecular Crystals and Molecules*. New York: Academic Press.
Kramer, R., Lehn, J. M. & Marquis-Rigault, A. (1993). *Proc. Natl Acad. Sci. USA*, **90**, 5394–5398.
Legrand, Y. M., van der Lee, A., Masquelez, N., Rabu, P. & Barboiu, M. (2007). *Inorg. Chem.* **46**, 9083–9089.
Lehn, J. (1999). *Chem. Eur. J.* **5**, 2455–2463.
Macrae, C. F., Bruno, I. J., Chisholm, J. A., Edgington, P. R., McCabe, P., Pidcock, E., Rodriguez-Monge, L., Taylor, R., van de Streek, J. & Wood, P. A. (2008). *J. Appl. Cryst.* **41**, 466–470.
Metrangolo, P., Meyer, F., Pilati, T., Resnati, G. & Terraneo, G. (2008). *Angew. Chem. Int. Ed.* **47**, 6114–6127.
Metrangolo, P., Pilati, T., Terraneo, G., Biella, S. & Resnati, G. (2009). *CrystEngComm*, **11**, 1187–1196.
Metrangolo, P., Präsang, C., Resnati, G., Liantonio, R., Whitwood, A. C. & Bruce, D. W. (2006). *Chem. Commun.* **31**, 3290–3292.
Metrangolo, P. & Resnati, G. (2001). *Chem. Eur. J.* **7**, 2511–2519.
Meyer, F. & Dubois, P. (2013). *CrystEngComm*, doi: 10.1039/C2CE26150B.
Nguyen, H. L., Horton, P. N., Hursthouse, M. B., Legon, A. C. & Bruce, D. W. (2004). *J. Am. Chem. Soc.* **126**, 16–17.
Ojala, W. H., Skrypek, T. M., MacQueen, B. C. & Ojala, C. R. (2010). *Acta Cryst.* C**66**, o565–o570.
Ouvrard, C., Le Questel, J.-Y., Berthelot, M. & Laurence, C. (2003). *Acta Cryst.* B**59**, 512–526.
Palatinus, L. & Chapuis, G. (2007). *J. Appl. Cryst.* **40**, 786–790.
Parisini, E., Metrangolo, P., Pilati, T., Resnati, G. & Terraneo, G. (2011). *Chem. Soc. Rev.* **40**, 2267–2278.
Politzer, P., Riley, K. E., Bulat, F. A. & Murray, J. S. (2012). *Comput. Theor. Chem.* **998**, 2–8.
Präsang, C., Whitwood, A. C. & Bruce, D. W. (2008). *Chem. Commun.* **18**, 2137–2139.
Raatikainen, K., Cametti, M. & Rissanen, K. (2010). *Beilstein J. Org. Chem.* **6**, doi: 10.3762/bjoc.6.4.
Ramasubbu, N., Parthasarathy, R. & Murray-Rust, P. (1986). *J. Am. Chem. Soc.* **108**, 4308–4314.
Rissanen, K. (2008). *CrystEngComm*, **10**, 1107–1113.
Saha, B. K. & Nangia, A. (2007). *Heteroat. Chem.* **18**, 185–194.
Sluis, P. van der & Spek, A. L. (1990). *Acta Cryst.* A**46**, 194–201.
Spek, A. L. (2003). *J. Appl. Cryst.* **36**, 7–13.
Storm, O. & Luning, J. (2002). *Chem. Eur. J.* **8**, 793–798.
Vance, A. L., Alcock, N. W., Heppert, J. A. & Busch, D. H. (1998). *Inorg. Chem.* **37**, 6912–6920.
Veljković, D. Ž., Janjić, G. V. & Zarić, S. D. (2011). *CrystEngComm*, **13**, 5005–5010.
Walter, S. M., Kniep, F., Herdtweck, E. & Huber, S. M. (2011). *Angew. Chem. Int. Ed.* **50**, 7187–7191.